nature neuroscience

Neuropeptide feedback modifies odor-evoked dynamics in *Caenorhabditis elegans* olfactory neurons

Sreekanth H Chalasani[1], Saul Kato[1,2], Dirk R Albrecht[1], Takao Nakagawa[1], L F Abbott[2] & Cornelia I Bargmann[1]

Many neurons release classical transmitters together with neuropeptide co-transmitters whose functions are incompletely understood. Here we define the relationship between two transmitters in the olfactory system of *C. elegans*, showing that a neuropeptide-to-neuropeptide feedback loop alters sensory dynamics in primary olfactory neurons. The AWC olfactory neuron is glutamatergic and also expresses the peptide NLP-1. Worms with *nlp-1* mutations show increased AWC-dependent behaviors, suggesting that NLP-1 limits the normal response. The receptor for NLP-1 is the G protein-coupled receptor NPR-11, which acts in postsynaptic AIA interneurons. Feedback from AIA interneurons modulates odor-evoked calcium dynamics in AWC olfactory neurons and requires INS-1, a neuropeptide released from AIA. The neuropeptide feedback loop dampens behavioral responses to odors on short and long timescales. Our results point to neuronal dynamics as a site of behavioral regulation and reveal the ability of neuropeptide feedback to remodel sensory networks on multiple timescales.

Embedded in an animal's neuroanatomy are the pathways that drive its behavior. More than twenty years ago, a wiring diagram of the *C. elegans* nervous system was constructed from serial-section electron micrographs[1]. Despite this unique resource, the relationships between sensory inputs, neuronal activity and specific behavioral programs in *C. elegans* are unclear[2,3]. We are exploring these issues within a circuit that generates undirected search when worms are removed from food, and directed chemotaxis in odor gradients[4–6]. Both of these behaviors are initiated by AWC olfactory neurons and are based on temporally regulated turning: in the absence of food, a transient bout of turning produces undirected local search; and in the presence of an odor gradient, temporally regulated turning produces a biased random walk for gradient climbing[7,8]. Through cell ablation and quantitative behavioral analysis, neurons in this circuit have been traced from sensory input to motor output[5,6]. Sensory neurons detect changes in odor levels or feeding state, and make synapses onto a layer of interneurons that control turning rates in a coordinated fashion; a second layer of interneurons and downstream motor neurons regulate specific classes of turns and features of turns. The turning circuit has interesting temporal properties. First, even in a constant odor environment, an intrinsic process generates apparently stochastic turns. Second, to move up a spatial odor gradient using a biased random walk, worms calculate the time derivative of the odor signal over seconds. Third, odor history and food regulate the overall turning rate on a longer timescale of minutes. A meaningful understanding of this circuit must include neuronal properties that represent these varied behavioral timescales.

RESULTS

The neuropeptide gene *nlp-1* limits local search behavior

The AWC neuron releases the neurotransmitter glutamate, which activates AIB interneurons via the glutamate-gated cation channel GLR-1 and inhibits AIY interneurons via the glutamate-gated chloride channel GLC-3 (ref. 9) (**Fig. 1a**). AWC also expresses genes that encode predicted neuropeptides, including the buccalin-related peptide NLP-1 (ref. 10). We characterized the function of NLP-1 by examining local search behavior, in which worms increase their turning rates during the initial 15 min after they are removed from food. Local search depends on AWC activity, and the rate of turning provides a quantitative measurement of AWC signaling[6]. A null mutant for *nlp-1*, generously provided by the *C. elegans* knockout consortium, had a higher turning rate than wild-type worms during local search (**Fig. 1b**). Like wild-type worms, *nlp-1* mutants stopped turning after 15 min off food (**Supplementary Table 1**). This behavioral profile suggests that *nlp-1* inhibits AWC-induced turning behavior.

NLP-1 reporter genes are expressed in AWC, ASI, PHB and BDU neurons and in the intestine[10]. The enhanced turning defect in *nlp-1* mutants was rescued by transgenic expression of *nlp-1* in AWC neurons, but not by expression in ASI neurons (**Fig. 1b** and **Supplementary Table 1**). Overexpression of *nlp-1* in AWC neurons of wild-type worms reduced the turning rate during local search (**Fig. 1b**). The opposite effects of *nlp-1* null mutants and gain-of-function transgenes suggest that this neuropeptide can be an instructive determinant of turning rates.

AWC-dependent turning behavior is reduced in worms with mutations in the vesicular glutamate transporter gene *eat-4* or in the glutamate receptors *glr-1* or *glc-3*; these defects are the opposite of those in *nlp-1* mutants[9]. Double mutants between *nlp-1* and *eat-4*, *glr-1* or *glc-3* had reduced turning rates, resembling the worms in which mutations affected glutamate signaling (**Fig. 1b**). This result suggests that NLP-1 functions as a co-transmitter whose effects are apparent only when the classical transmitter glutamate is also released: glutamate from AWC stimulates turning, and NLP-1 from AWC decreases the magnitude of this effect.

[1]Howard Hughes Medical Institute, The Rockefeller University, New York, New York, USA. [2]Department of Neuroscience, Department of Physiology and Cellular Biophysics, Columbia University College of Physicians and Surgeons, New York, New York, USA. Correspondence should be addressed to C.I.B. (cori@rockefeller.edu).

Received 29 October 2009; accepted 23 February 2010; published online 4 April 2010; doi:10.1038/nn.2526

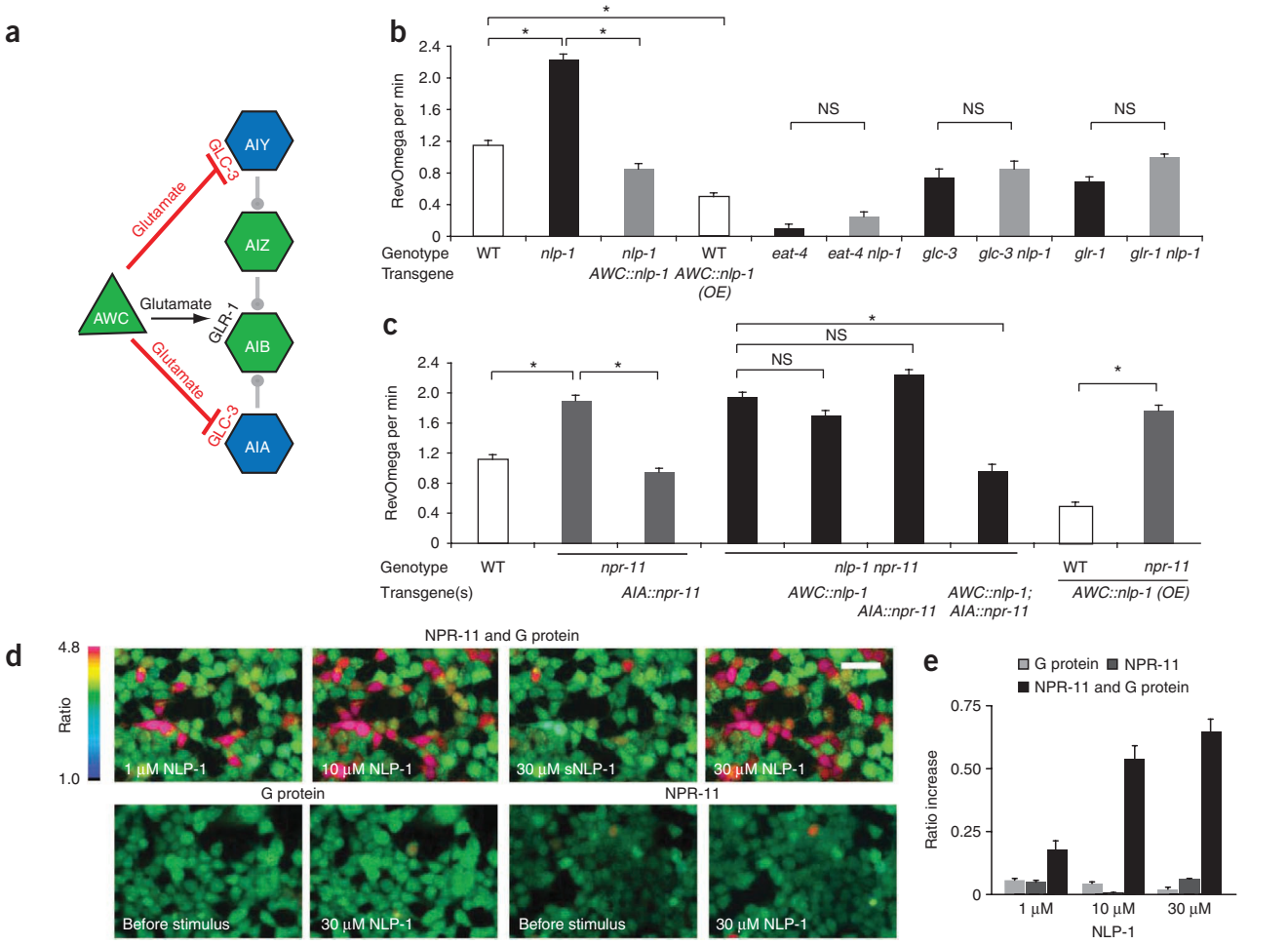

Figure 1 AWC releases NLP-1, which acts on NPR-11 in AIA. (**a**) AWC sensory neurons, downstream interneurons, and relevant glutamate receptors (from this work (AIA) and ref. 9). (**b**,**c**) Local search behavior 7–12 min after removal from food. RevOmega, coupled reversal-omega behaviors characteristic of local search. Analysis of *nlp-1* mutants (**b**) and *npr-11* mutants (**c**). In all figures, WT indicates control N2 strain, *AWC::nlp-1* indicates *nlp-1* cDNA under AWC-selective *odr-3* promoter, *AWC::nlp-1(OE)* indicates the same plasmid injected at high concentrations, *AIA::npr-11* indicates *npr-11* cDNA under AIA-selective *gcy-28.d* promoter. Error bars, s.e.m.; $*P < 0.05$ by *t*-test or *t*-test with Bonferroni correction, as appropriate; NS, not significant. Complete behavioral data with all genotypes and time points are in **Supplementary Table 1**. (**d**,**e**) Response of *npr-11*- and Gα16Z-, *npr-11* or Gα16Z- transfected HEK 293 cells to an NLP-1 peptide and a scrambled NLP-1 peptide (sNLP-1). (**d**) Pseudocolor images of fura2-labeled cells indicating fluorescent ratio intensities. Scale bar, 100 μm. (**e**) Average calcium response of all cells in the window ($n = 10$ fields for *npr-11* and Gα16Z, $n = 8$ for *npr-11* and $n = 7$ for Gα16Z). Means and s.e.m. are shown.

NLP-1 acts through the G protein-coupled receptor NPR-11

The *C. elegans* genome encodes ~100 G protein–coupled receptors (GPCRs) related to characterized neuropeptide receptors (http://www.wormbase.org/). To identify the receptor for NLP-1, we examined GPCRs that lack known ligands, focusing on those that are expressed in neurons connected to AWC[11,12]. The orphan GPCR NPR-11, whose closest characterized homolog is the *Drosophila* neuropeptide F receptor 1, was one candidate. We found that *npr-11* null mutants, like *nlp-1* mutants, had increased turning during AWC-dependent local search behavior (**Fig. 1c** and **Supplementary Table 1**).

Worms with double *nlp-1 npr-11* mutations resembled the single mutants in turning behavior, as expected for a ligand-receptor pair that acts together and not additively (**Fig. 1c**). In addition, the *npr-11* mutation fully suppressed the effects of *nlp-1* overexpression on turning behavior (**Fig. 1c**). This result indicates that *npr-11* is necessary for the biological activity of *nlp-1*, as predicted if *npr-11* encodes an *nlp-1* receptor.

Reporter genes for *npr-11* are expressed in two postsynaptic targets of AWC, the AIA and AIY interneurons, and in other neurons[11] (data not shown). The *npr-11* behavioral defect in local search behavior resembled the defect after AIA interneurons are killed with a laser[9], and the *npr-11* defect was fully rescued by transgenic *npr-11* expression in AIA interneurons under the *gcy-28.d* promoter (**Fig. 1c**). These results suggest that release of NLP-1 from AWC neurons activates the NPR-11 GPCR on AIA neurons. In agreement with this hypothesis, the turning behavior of *nlp-1 npr-11* double mutants was rescued only when *nlp-1* was expressed in AWC and *npr-11* was expressed in AIA together in the same strain (**Fig. 1c** and **Supplementary Table 1**).

We obtained a biochemical confirmation of the genetically inferred ligand-receptor relationship for NLP-1 and NPR-11 by expressing NPR-11 in HEK 293 cells together with the promiscuous G protein α16Z[13], and exposing the cells to synthesized MDANAFRMSFamide, an amidated peptide corresponding to one of four predicted peptides encoded by *nlp-1*, MDANAFRMSFamide. NPR-11-expressing cells responded to micromolar concentrations of the peptide with calcium

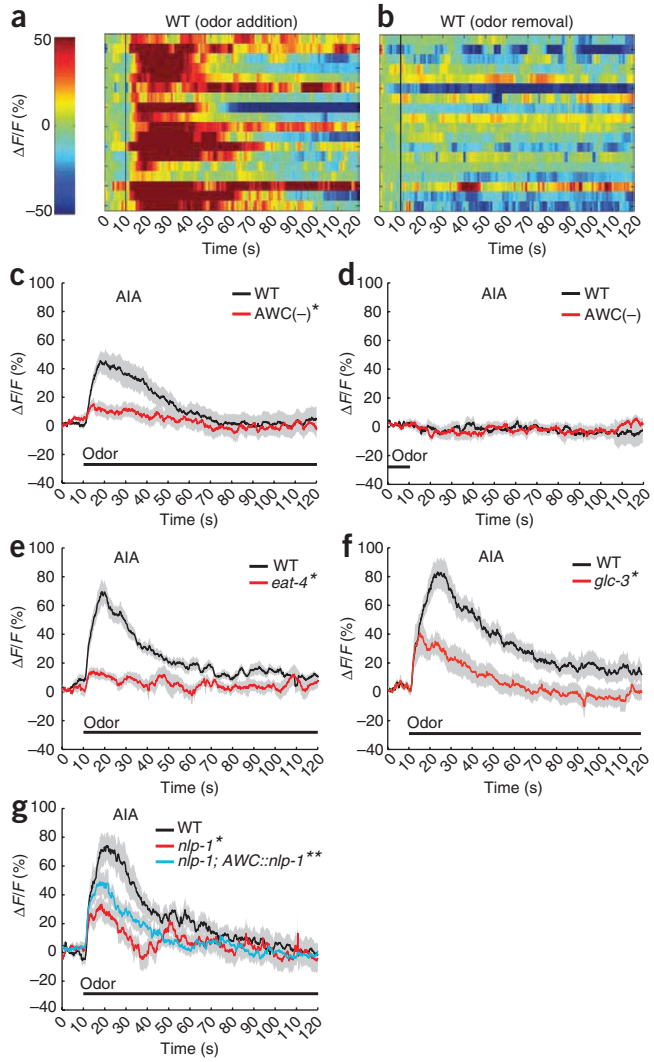

Figure 2 Calcium responses in AIA interneurons require AWC glutamate and NLP-1. (**a**,**b**) Heat maps showing the ratio of change in fluorescence to total fluorescence in AIA neurons expressing GCaMP2.2b[15]; addition (**a**) and removal (**b**) of odor stimulus at $t = 10$ s in each recording ($n = 18$). (**c**,**d**) Average G-CaMP fluorescence change in AIA neurons in wild-type (WT; $n = 18$) and wild-type AWC-ablated worms ($n = 12$) on addition (**c**) and removal (**d**) of odor. (**e**–**g**) Mutant AIA responses. (**e**) *eat-4* ($n = 18$, WT $n = 18$). (**f**) *glc-3* ($n = 16$, WT $n = 16$). (**g**) *nlp-1* ($n = 18$, WT $n = 18$) and *AWC::nlp-1* cell-selective rescue ($n = 18$). In all imaging figures, odor is a 10^{-4} dilution of isoamyl alcohol. Light gray shading indicates s.e.m. *Significantly different from wild type; **significantly different from *nlp-1* mutant ($P < 0.05$, *t*-test with Bonferroni correction).

transients typical for GPCR activation (**Fig. 1d**). We observed no responses to scrambled NLP-1 peptide in untransfected cells or in cells expressing the receptor or G protein alone (**Fig. 1d**,**e**).

AWC inhibits AIA interneurons through glutamate and NLP-1

We investigated the relationship between AWC and AIA interneurons using genetically encoded calcium indicators of the G-CaMP family, which emit increased fluorescence upon calcium binding[14,15]. *C. elegans* neurons are thought to lack sodium-based action potentials, but express voltage-gated calcium channels[16], and calcium signals in these neurons correlate with neuronal depolarization[17–22]. Previous results suggest that AWC neurons have basal activity at rest, are hyperpolarized by addition of odors and are strongly activated by odor removal[9]. We found that AIA interneurons had the opposite response, showing large transient calcium increases upon odor addition (**Fig. 2a**,**b**). Odor responses in AIA required sensory input from AWC, as they were strongly attenuated when AWC neurons were killed using a laser microbeam (**Fig. 2c**,**d**). These results suggest that AWC forms inhibitory synapses onto AIA, as suggested for the synapses between AWC and AIY (**Fig. 1a**)[9]. In the simplest model, basal AWC activity at rest tonically inhibits AIA; when odor is added, AWC is hyperpolarized, tonic inhibition of AIA is reduced, and AIA becomes active.

Both glutamate and NLP-1 contributed to odor-evoked calcium responses in AIA. AIA responses to odor were diminished in *eat-4* mutants that lack the vesicular glutamate transporter and in *glc-3* mutants that lack a glutamate-gated chloride channel (**Fig. 2e**,**f**). The involvement of *glc-3* is consistent with its known expression in AIA, its molecular identity as an inhibitory glutamate-gated channel, and the prediction that the AWC-to-AIA synapse is inhibitory[11,23]. Worms with mutations in *nlp-1* also had a diminished response in AIA interneurons, which was partly rescued by expression of *nlp-1* in AWC neurons (**Fig. 2g**). The partial rescue of *nlp-1* may be due to variable expression of transgenes or to a combined action of *nlp-1* in AWC and additional neurons.

Although a dual action of glutamate and NLP-1 on AIA calcium signals was consistent with the behavioral analysis, the relationship between the transmitters was unexpected. In turning behavior, glutamate and NLP-1 had opposite effects, but in AIA calcium imaging experiments, the effects of *nlp-1* and *glc-3* were congruent. This distinction suggests that the behavioral effect of NLP-1 cannot be entirely explained by its observed effect on AIA activity, and prompted further examination of neurons in the AWC circuit.

AWC responses are modulated by NLP-1

The activity of sensory neurons such as AWC is thought to be defined primarily by sensory input and not by network interactions. Unexpectedly, calcium imaging of the odor-evoked response in AWC neurons revealed alterations in *nlp-1* mutants. In both wild-type and *nlp-1* worms, initial calcium responses to odor removal peaked within 10 s of odor removal (**Fig. 3a–c** and **Supplementary Figs. 1** and **2**). However, in *nlp-1* mutants, the first peak was frequently followed by large secondary calcium transients that continued for at least 2 min after odor removal, the longest duration that was practical for calcium imaging (**Fig. 3b**,**c**). Thus, NLP-1 signaling suppressed AWC calcium transients for a long period after odor removal.

To quantitatively describe the altered activity in *nlp-1* mutants, we used a discrete Fourier transform to analyze the temporal character of the AWC calcium response to odor removal. Fourier analysis is well suited to reveal oscillatory or repeating signals, which appeared by inspection to be present in traces from *nlp-1* mutants. Indeed, spectral analysis showed increased power in a mid-frequency domain in *nlp-1* mutants, with a significantly greater contribution than in the wild type from periodic components between 0.033 Hz and 1 Hz (period 1–30 s) (**Fig. 3d**). The effects were statistically detectable at all time points and suggest the presence of irregular slow oscillations with a preferred period near 20 s. Cell-selective transgenic expression of *nlp-1* in AWC resulted in partial but significant rescue of the defect (**Fig. 3c**,**d** and **Supplementary Fig. 1**). The irregular oscillating signal was not observed in the absence of odor, excluding trivial optical or mechanical artifacts (**Supplementary Fig. 1**), but it was observed to some degree in wild-type traces as well as *nlp-1* traces, indicating that it is a component of the normal AWC response.

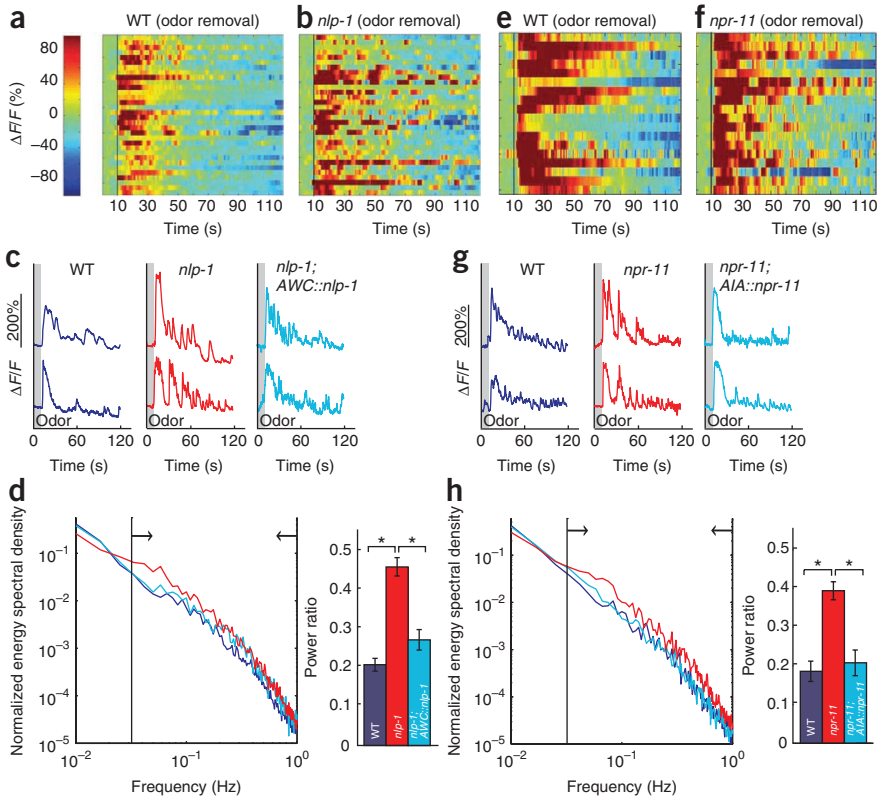

Figure 3 Altered AWC calcium responses in *nlp-1* and *npr-11* mutants. (**a**,**b**,**e**,**f**) Heat maps showing ratio change in fluorescence to total fluorescence in AWC neurons expressing G-CaMP1.0. Odor was removed at 10 s in each recording. (**a**) Wild type ($n = 32$); (**b**) *nlp-1* ($n = 32$); (**e**) wild type ($n = 18$); (**f**) *npr-11* ($n = 18$). (**c**,**g**) Representative AWC calcium responses from individual wild-type worms, *nlp-1* (**c**) and *npr-11* mutants (**g**), and rescued strains. (**d**,**h**) Fourier power analysis of AWC calcium responses in *nlp-1* (**d**) and *npr-11* mutants (**h**). Left, normalized energy density spectrum averaged across all calcium traces of each genotype; arrows indicate range of the middle frequency band (color code on right). Right, the average power ratio of the middle frequency band (0.033–1 Hz) across all calcium traces of each genotype; error bars, s.e.m. *$P < 0.05$ (*t*-test with Bonferroni correction).

We also observed enhanced secondary AWC calcium signals in *npr-11* mutants after odor removal (**Fig. 3e–g** and **Supplementary Figs. 1** and **2**). Normal AWC calcium signals were restored by transgenic expression of *npr-11* in AIA neurons (**Fig. 3g,h** and **Supplementary Fig. 1**). The functional effect of a receptor in AIA on odor responses in AWC supports the existence of feedback from AIA to AWC. In summary, these results suggest that release of NLP-1 from AWC, sensed by NPR-11 in AIA, results in feedback onto AWC that suppresses secondary calcium transients after odor removal.

If modulatory feedback from the circuit contributes to normal AWC activity, other synaptic mutants could also affect AWC odor responses. Indeed, AWC responses to odor removal were reduced in *eat-4* mutants, which lack glutamatergic transmission from AWC and other neurons, and prolonged in *unc-31* mutants, which have reduced neuropeptide release from all neurons[24,25] (**Supplementary Fig. 2c,d**). These results suggest that the long-lasting AWC responses to odor removal are affected by synaptic inputs, with positive inputs from glutamatergic neurons and negative inputs from peptidergic neurons.

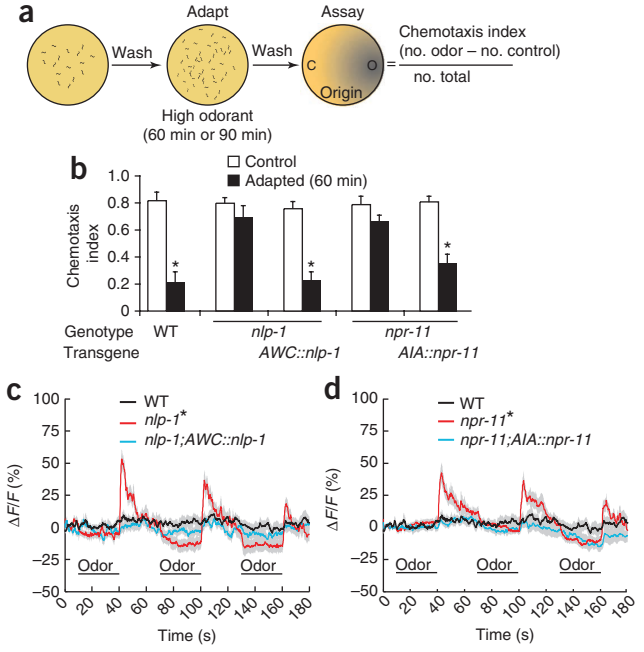

Figure 4 Worms with mutations in *nlp-1* and *npr-11* are defective in olfactory adaptation. (**a**) Schematic diagram of adaptation assay. (**b**) Adaptation in *nlp-1* and *npr-11* mutants, and cell-selective rescue. Error bars, s.e.m. *$P < 0.05$ (*t*-test with Bonferroni correction). (**c**,**d**) AWC calcium responses in wild-type, *nlp-1* and *AWC::nlp-1* transgenic rescued worms (**c**) and wild-type, *npr-11* and *AIA::npr-11* transgenic rescued worms (**d**) adapted for 60 min ($n = 12$ each). Odor pulses are marked. Light gray shading indicates s.e.m. *Significantly different from wild type ($P < 0.05$, *t*-test with Bonferroni correction).

nlp-1 mutants are defective in AWC odor adaptation

The results described above suggest that neuropeptide signaling and feedback influence long-lasting dynamics in AWC neurons. The 15-min local search behavior is one example of a sustained AWC-dependent behavior; a second sustained AWC-dependent behavior is olfactory adaptation, a behavioral change in which prolonged exposure to an odor leads to reduced chemotaxis to that odor[26] (**Fig. 4a,b**). Worms with mutations in *nlp-1* or *npr-11* failed to adapt to odors after a 60-min exposure (**Fig. 4b**), although they did adapt after a 90-min exposure (**Supplementary Fig. 3a**). Like the defects in local search behavior, the olfactory adaptation defects were rescued by transgenic expression of *nlp-1* in AWC and transgenic expression of *npr-11* in AIA, respectively (**Fig. 4b**).

Signaling components that are required cell-autonomously for olfactory adaptation in AWC include GPCR regulators, TRPV channels and a cyclic GMP–dependent protein kinase[27–32]. However, the effects of adaptation on AWC activity have not been described. We found that wild-type worms that had been adapted to odor for 60 min failed to respond to odor removal with AWC calcium transients, suggesting

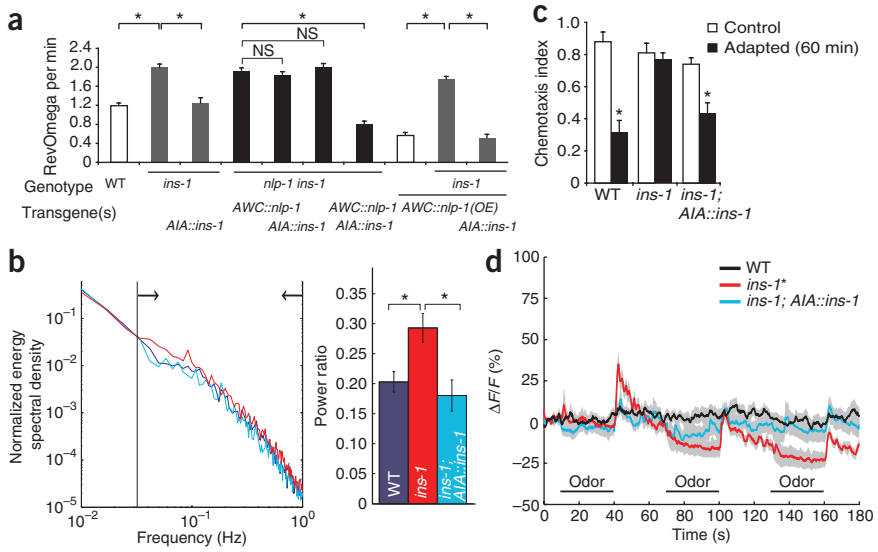

Figure 5 *ins-1* is a component of the *nlp-1-npr-11* pathway. (**a**) Local search behavior 7–12 min after removal from food. RevOmega, coupled reversal-omega behaviors characteristic of local search. *AIA::ins-1*, *ins-1* cDNA expressed under AIA-selective *gcy-28.d* promoter. Error bars, s.e.m. $^*P < 0.05$, *t*-test with Bonferroni correction. (**b**) Fourier power analysis of AWC calcium responses in *ins-1* mutants. Left, the normalized energy density spectrum averaged across all calcium traces of each genotype; arrows indicate range of the middle frequency band (color code on right). Right, the average power ratio of the middle frequency band (0.033–1 Hz) across all calcium traces of each genotype; error bars, s.e.m. $^*P < 0.05$ (*t*-test with Bonferroni correction). (**c**) Adaptation in *ins-1* mutants, and cell-selective rescue. *Different from unadapted control ($P < 0.05$, *t*-test). Error bars, s.e.m. (**d**) AWC calcium responses in wild-type, *ins-1* and *AIA::ins-1* rescued transgenic worms adapted for 60 min ($n = 12$ each). Odor pulses are marked. Light gray shading indicates s.e.m. *Different from wild type at $P < 0.05$, *t*-test with Bonferroni correction.

that adaptation blocked an early step of AWC signaling (**Fig. 4c**). By contrast, both *nlp-1* and *npr-11* mutants that had been exposed to odor for 60 min responded with AWC calcium transients after odor removal (**Fig. 4c,d**). Transgenic expression of *nlp-1* in AWC and *npr-11* in AIA neurons restored the wild-type AWC calcium response (**Fig. 4c,d**). These results indicate that NLP-1 release from AWC, acting on the NPR-11 receptor in AIA, generates feedback that reduces the primary AWC response to odor removal after adaptation.

INS-1 is a candidate feedback signal from AIA

The results described above suggest that AIA releases a signal that suppresses odor-evoked calcium responses in AWC. The insulin-related neuropeptide INS-1, which is expressed in AIA, modulates the function of the ASE gustatory neurons in a salt conditioning assay[33], suggesting that INS-1 is a candidate signal from AIA to sensory neurons. Therefore, we investigated the effects of *ins-1* mutations on AWC-regulated behaviors. Like *nlp-1* and *npr-11* mutants, *ins-1* mutants showed increased turning in AWC-dependent local search behavior (**Fig. 5a** and **Supplementary Table 1**). Double *ins-1 nlp-1* mutants resembled each single mutant, suggesting that these genes act in a common process (**Fig. 5a**). An *ins-1* mutation fully suppressed the effects of NLP-1 overexpression on turning behavior, indicating that *ins-1* activity is necessary for the biological effects of *nlp-1* (**Fig. 5a**).

Expression of *ins-1* is found in multiple neurons including AIA, RIC, ASI and AWC[33]. Transgenic expression of *ins-1* from an AIA-selective promoter rescued turning behavior in the *ins-1* mutant, but expression from AWC-, ASI- or RIC-selective promoters did not (**Fig. 5a** and **Supplementary Table 1** and data not shown). These results suggest that *ins-1* is required in AIA neurons. In double mutant studies, *nlp-1 ins-1* mutants were restored to normal turning behavior only when *nlp-1* was expressed in AWC and *ins-1* was also expressed in AIA (**Fig. 5a**). Double *nlp-1 (overexpressor) ins-1* mutants were restored to the behavior of *nlp-1(overexpressor)* strains when *ins-1* was expressed in AIA (**Fig. 5a**). These experiments support the idea that *ins-1* acts in AIA neurons.

In calcium imaging experiments, *ins-1* mutants had secondary AWC transients after odor removal, with temporal properties similar to *nlp-1* and *npr-11* mutants (**Fig. 5b** and **Supplementary Fig. 4**). AIA-specific expression of *ins-1* significantly rescued the altered odor response in AWC neurons, suggesting that AIA neuropeptides influence AWC activity (**Fig. 5b** and **Supplementary Fig. 4**).

AWC-dependent olfactory adaptation also required *ins-1*. Like *nlp-1* and *npr-11* mutants, *ins-1* mutants did not adapt after a 60-min exposure to odor but did adapt partially after 90-min (**Fig. 5c** and **Supplementary Fig. 3**). Adaptation in *nlp-1 ins-1* double mutants was similar to adaptation in each single mutant, suggesting that these two genes affect a common pathway (**Supplementary Fig. 3c**). Moreover, AWC neurons in *ins-1* mutants exposed to odors for 60 min showed a calcium response after odor removal, unlike wild-type worms in the same conditions (**Fig. 5d**). Both the behavioral adaptation and the neuronal correlate of adaptation observed in calcium imaging were rescued by transgenic expression of *ins-1* in AIA (**Fig. 5c,d** and **Supplementary Fig. 3**). These results suggest that INS-1 released from AIA acts directly or indirectly on AWC sensory neurons to limit their activity.

DISCUSSION

Many neurons release both classical neurotransmitters and neuropeptides[34–36]. Our results suggest that AWC releases both the classical neurotransmitter glutamate and the neuropeptide NLP-1 to modulate behavior (**Supplementary Fig. 4e**). The glutamate signaling pathway promotes local search and odor chemotaxis, whereas the neuropeptide pathway limits local search and promotes odor adaptation. Glutamate signals are interpreted by multiple glutamate receptors on interneurons[9], and NLP-1 is sensed by NPR-11 on AIA interneurons. These interneurons then release INS-1, which directly or indirectly limits AWC activity and behavior. In one straightforward model, INS-1 is released from active AIA neurons when odor is present; the INS-1 released during a short odor exposure inhibits repetitive calcium transients from AWC neurons when odor is removed, and the prolonged INS-1 release during a long odor exposure has a stronger effect, completely suppressing AWC calcium transients upon subsequent odor removal. This feedback loop may act as a gain control circuit to dampen the responses of AWC neurons to strong stimuli, like negative feedback in other neuronal systems[37]. In this interpretation, the increased oscillations in *nlp-1* and other mutants result from ungoverened high-gain signaling in AWC.

A number of inhibitory pathways involving a single neuropeptide are known; this pathway is unusual in its apparent requirement for

two neuropeptides from two neurons, working in a feedback loop. Several properties of this feedback loop remain to be determined. For example, we do not know when NLP-1 and INS-1 are released with respect to food or odor cues, and with respect to AWC and AIA activity. If the peptides are released when the neurons are active, NLP-1 would be released in alternation with INS-1 and not simultaneously; the slow biochemical timescale of G protein signaling may permit temporal integration across asynchronous activity of AWC and AIA[38]. Another missing component of the feedback model is the receptor for INS-1, as mutation of the one characterized *C. elegans* insulin receptor gene, *daf-2*, did not mimic or suppress *ins-1* mutations as predicted for an *ins-1* receptor (data not shown). INS-1 antagonizes DAF-2 in the developmental dauer larva pathway[39], and can act either as an agonist or an antagonist of DAF-2 in food-regulated thermal learning and salt learning paradigms[33,40], but *C. elegans* has more than 30 insulin-regulated peptides, and DAF-2 may not be the only receptor for this peptide family. Precedent for alternative insulin receptors exists in mammals, where GPCRs are receptors for the insulin-related relaxin peptides[41].

The behavioral functions of INS-1 in AWC olfactory adaptation are related to its functions during ASE salt chemotaxis learning, where INS-1 from AIA suppresses chemotaxis after salt is paired with starvation[33]. It will be interesting to investigate whether NLP-1 or another sensory peptide initiates ASE salt chemotaxis learning, and whether INS-1 signaling alters ASE sensory dynamics. Although we specifically examined the relationship between AWC and AIA, the AIA interneurons also receive synaptic input from neurons that sense food, tastants, pheromones and repellents[1,33,42]. This connectivity might enable AIA to act as a local integrator of sensory information.

There is increasing evidence that peripheral olfactory signaling in many species is modulated by top-down signals, internal states and neuromodulators. State-dependent inputs affect olfactory signaling in rodents, acting as early as the synapses of the olfactory sensory neurons[43,44]. In *Drosophila*, tachykinin peptides expressed by local interneurons mediate presynaptic inhibition of olfactory receptor neurons[45]. The modulation of primary sensory neurons is a prominent feature of pain-sensing pathways[46]; we suggest that it will also be prominent in olfactory systems. In *C. elegans*, the use of specific mutants allows these feedback mechanisms to be directly linked to olfactory responses and behaviors, and also reveals their functional diversity. The neuropeptide feedback loop described here damps AWC output, whereas a different modulatory pathway involving the receptor guanylate cyclase GCY-28 can regulate an AWC switch from behavioral attraction to repulsion[8]. The *C. elegans* genome contains about 113 genes that encode more than 250 predicted neuropeptides, a rich potential source of behavioral variability[10,47,48].

Our experiments reveal neuropeptide-regulated dynamic properties of *C. elegans* neurons that correlate with the dynamics of behavior. The prolonged AWC calcium signals in *nlp-1*, *npr-11* and *ins-1* mutants correlate with their increased turning during local search behavior. The reduced AWC calcium signals after prolonged odor exposure correlate with olfactory adaptation, which is reduced in *nlp-1*, *npr-11* and *ins-1* mutants. Further studies of the AWC circuit should generate a better understanding of the relationship between behavior and the time-varying acute responses of AIA, sustained responses of AIB, and repetitive responses of AWC and AIY[9]. Together with previous findings in *C. elegans* mechanosensory neurons[49], these results suggest that circuit input tunes sensory responses to external stimuli based on sensory history and internal states, generating a rudimentary form of decision making.

METHODS

Methods and any associated references are available in the online version of the paper at http://www.nature.com/natureneuroscience/.

Note: Supplementary information is available on the Nature Neuroscience website.

ACKNOWLEDGMENTS

We thank the *C. elegans* knockout consortium and the Caenorhabditis Genetic Center (CGC) for strains, Y.H. Wang for the α16Z chimera, L. Looger for GCaMP2.2b, Y. Iino for discussions about *ins-1*, and L. Vosshall, G. Lee, E. Feinberg, M. Tsunozaki, J. Gray, J. Garrison, P. McGrath and members of the Bargmann laboratory for critical help, advice and insights. Peptide synthesis was performed by the Proteomics Resource Center of the Rockefeller University. This work was funded by the Mathers Foundation and by the Howard Hughes Medical Institute (C.I.B.). D.R.A. holds a Career Award at the Scientific Interface from the Burroughs Wellcome Fund.

AUTHOR CONTRIBUTIONS

S.H.C. conceived, conducted and interpreted experiments and co-wrote the paper; S.K., D.R.A. and L.F.A. performed and interpreted data analysis; T.N. performed HEK expression experiments; C.I.B. conceived and interpreted experiments and co-wrote the paper.

COMPETING FINANCIAL INTERESTS

The authors declare no competing financial interests.

Published online at http://www.nature.com/natureneuroscience/.
Reprints and permissions information is available online at http://npg.nature.com/reprintsandpermissions/.

1. White, J.G., Southgate, E., Thomson, J.N. & Brenner, S. The structure of the nervous system of the nematode *Caenorhabditis elegans*. *Phil. Transact. R. Soc. Lond. B* **314**, 1–340 (1986).
2. Chalfie, M. *et al.* The neural circuit for touch sensitivity in *Caenorhabditis elegans*. *J. Neurosci.* **5**, 956–964 (1985).
3. Bargmann, C.I. Chemosensation in *C. elegans*. in *WormBook* (ed. The *C. elegans* Research Community) doi:10.1895/wormbook.1.123.1, <http://www.wormbook.org> (2006).
4. Bargmann, C.I., Hartwieg, E. & Horvitz, H.R. Odorant-selective genes and neurons mediate olfaction in *C. elegans*. *Cell* **74**, 515–527 (1993).
5. Wakabayashi, T., Kitagawa, I. & Shingai, R. Neurons regulating the duration of forward locomotion in *Caenorhabditis elegans*. *Neurosci. Res.* **50**, 103–111 (2004).
6. Gray, J.M., Hill, J.J. & Bargmann, C.I. A circuit for navigation in *Caenorhabditis elegans*. *Proc. Natl. Acad. Sci. USA* **102**, 3184–3191 (2005).
7. Pierce-Shimomura, J.T., Morse, T.M. & Lockery, S.R. The fundamental role of pirouettes in *Caenorhabditis elegans* chemotaxis. *J. Neurosci.* **19**, 9557–9569 (1999).
8. Tsunozaki, M., Chalasani, S.H. & Bargmann, C.I. A behavioral switch: cGMP and PKC signaling in olfactory neurons reverses odor preference in *C. elegans*. *Neuron* **59**, 959–971 (2008).
9. Chalasani, S.H. *et al.* Dissecting a circuit for olfactory behaviour in *Caenorhabditis elegans*. *Nature* **450**, 63–70 (2007).
10. Nathoo, A.N., Moeller, R.A., Westlund, B.A. & Hart, A.C. Identification of neuropeptide-like protein gene families in *Caenorhabditis elegans* and other species. *Proc. Natl. Acad. Sci. USA* **98**, 14000–14005 (2001).
11. Wenick, A.S. & Hobert, O. Genomic cis-regulatory architecture and trans-acting regulators of a single interneuron-specific gene battery in *C. elegans*. *Dev. Cell* **6**, 757–770 (2004).
12. Etchberger, J.F. *et al.* The molecular signature and cis-regulatory architecture of a *C. elegans* gustatory neuron. *Genes Dev.* **21**, 1653–1674 (2007).
13. Mody, S.M., Ho, M.K., Joshi, S.A. & Wong, Y.H. Incorporation of Galpha(z)-specific sequence at the carboxyl terminus increases the promiscuity of galpha(16) toward G(i)-coupled receptors. *Mol. Pharmacol.* **57**, 13–23 (2000).
14. Tallini, Y.N. *et al.* Imaging cellular signals in the heart in vivo: Cardiac expression of the high-signal Ca2+ indicator GCaMP2. *Proc. Natl. Acad. Sci. USA* **103**, 4753–4758 (2006).
15. Tian, L. *et al.* Imaging neural activity in worms, flies and mice with improved GCaMP calcium indicators. *Nat. Methods* **6**, 875–881 (2009).
16. Lockery, S.R. & Goodman, M.B. The quest for action potentials in *C. elegans* neurons hits a plateau. *Nat. Neurosci.* **12**, 377–378 (2009).
17. Suzuki, H. *et al.* In vivo imaging of *C. elegans* mechanosensory neurons demonstrates a specific role for the MEC-4 channel in the process of gentle touch sensation. *Neuron* **39**, 1005–1017 (2003).
18. O'Hagan, R., Chalfie, M. & Goodman, M.B. The MEC-4 DEG/ENaC channel of *Caenorhabditis elegans* touch receptor neurons transduces mechanical signals. *Nat. Neurosci.* **8**, 43–50 (2005).
19. Clark, D.A., Biron, D., Sengupta, P. & Samuel, A.D. The AFD sensory neurons encode multiple functions underlying thermotactic behavior in *Caenorhabditis elegans*. *J. Neurosci.* **26**, 7444–7451 (2006).

20. Ramot, D., MacInnis, B.L. & Goodman, M.B. Bidirectional temperature-sensing by a single thermosensory neuron in *C. elegans*. *Nat. Neurosci.* **11**, 908–915 (2008).
21. Mellem, J.E., Brockie, P.J., Zheng, Y., Madsen, D.M. & Maricq, A.V. Decoding of polymodal sensory stimuli by postsynaptic glutamate receptors in *C. elegans*. *Neuron* **36**, 933–944 (2002).
22. Chronis, N., Zimmer, M. & Bargmann, C.I. Microfluidics for *in vivo* imaging of neuronal and behavioral activity in *Caenorhabditis elegans*. *Nat. Methods* **4**, 727–731 (2007).
23. Horoszok, L., Raymond, V., Sattelle, D.B. & Wolstenholme, A.J. GLC-3: a novel fipronil and BIDN-sensitive, but picrotoxinin-insensitive, L-glutamate-gated chloride channel subunit from *Caenorhabditis elegans*. *Br. J. Pharmacol.* **132**, 1247–1254 (2001).
24. Lee, R.Y., Sawin, E.R., Chalfie, M., Horvitz, H.R. & Avery, L. EAT-4, a homolog of a mammalian sodium-dependent inorganic phosphate cotransporter, is necessary for glutamatergic neurotransmission in *Caenorhabditis elegans*. *J. Neurosci.* **19**, 159–167 (1999).
25. Sieburth, D., Madison, J.M. & Kaplan, J.M. PKC-1 regulates secretion of neuropeptides. *Nat. Neurosci.* **10**, 49–57 (2007).
26. Colbert, H.A. & Bargmann, C.I. Odorant-specific adaptation pathways generate olfactory plasticity in *C. elegans*. *Neuron* **14**, 803–812 (1995).
27. Colbert, H.A., Smith, T.L. & Bargmann, C.I. OSM-9, a novel protein with structural similarity to channels, is required for olfaction, mechanosensation, and olfactory adaptation in *Caenorhabditis elegans*. *J. Neurosci.* **17**, 8259–8269 (1997).
28. L'Etoile, N.D. *et al.* The cyclic GMP-dependent protein kinase EGL-4 regulates olfactory adaptation in *C. elegans*. *Neuron* **36**, 1079–1089 (2002).
29. Palmitessa, A. *et al. Caenorhabditis elegans* arrestin regulates neural G protein signaling and olfactory adaptation and recovery. *J. Biol. Chem.* **280**, 24649–24662 (2005).
30. Matsuki, M., Kunitomo, H. & Iino, Y. Goalpha regulates olfactory adaptation by antagonizing Gqalpha-DAG signaling in *Caenorhabditis elegans*. *Proc. Natl. Acad. Sci. USA* **103**, 1112–1117 (2006).
31. Yamada, K., Hirotsu, T., Matsuki, M., Kunitomo, H. & Iino, Y. GPC-1, a G protein gamma-subunit, regulates olfactory adaptation in *Caenorhabditis elegans*. *Genetics* **181**, 1347–1357 (2009).
32. Kaye, J.A., Rose, N.C., Goldsworthy, B., Goga, A. & L'Etoile, N.D. A 3′UTR pumilio-binding element directs translational activation in olfactory sensory neurons. *Neuron* **61**, 57–70 (2009).
33. Tomioka, M. *et al.* The insulin/PI 3-kinase pathway regulates salt chemotaxis learning in *Caenorhabditis elegans*. *Neuron* **51**, 613–625 (2006).
34. Marder, E. & Bucher, D. Understanding circuit dynamics using the stomatogastric nervous system of lobsters and crabs. *Annu. Rev. Physiol.* **69**, 291–316 (2007).
35. Nassel, D.R. & Homberg, U. Neuropeptides in interneurons of the insect brain. *Cell Tissue Res.* **326**, 1–24 (2006).
36. Burnstock, G. Cotransmission. *Curr. Opin. Pharmacol.* **4**, 47–52 (2004).
37. Demb, J.B. Functional circuitry of visual adaptation in the retina. *J. Physiol. (Lond.)* **586**, 4377–4384 (2008).
38. Stein, W., DeLong, N.D., Wood, D.E. & Nusbaum, M.P. Divergent co-transmitter actions underlie motor pattern activation by a modulatory projection neuron. *Eur. J. Neurosci.* **26**, 1148–1165 (2007).
39. Pierce, S.B. *et al.* Regulation of DAF-2 receptor signaling by human insulin and ins-1, a member of the unusually large and diverse *C. elegans* insulin gene family. *Genes Dev.* **15**, 672–686 (2001).
40. Kodama, E. *et al.* Insulin-like signaling and the neural circuit for integrative behavior in *C. elegans*. *Genes Dev.* **20**, 2955–2960 (2006).
41. Ivell, R. & Einspanier, A. Relaxin peptides are new global players. *Trends Endocrinol. Metab.* **13**, 343–348 (2002).
42. Macosko, E.Z. *et al.* A hub-and-spoke circuit drives pheromone attraction and social behaviour in *C. elegans*. *Nature* **458**, 1171–1175 (2009).
43. Wachowiak, M., Wesson, D.W., Pirez, N., Verhagen, J.V. & Carey, R.M. Low-level mechanisms for processing odor information in the behaving animal. *Ann. NY Acad. Sci.* **1170**, 286–292 (2009).
44. Gomez, C. *et al.* Heterogeneous targeting of centrifugal inputs to the glomerular layer of the main olfactory bulb. *J. Chem. Neuroanat.* **29**, 238–254 (2005).
45. Ignell, R. *et al.* Presynaptic peptidergic modulation of olfactory receptor neurons in *Drosophila*. *Proc. Natl. Acad. Sci. USA* **106**, 13070–13075 (2009).
46. Stein, C. *et al.* Peripheral mechanisms of pain and analgesia. *Brain Res. Brain Res. Rev.* **60**, 90–113 (2009).
47. Li, C. & Kim, K. Neuropeptides. in *WormBook* (ed. The *C. elegans* Research Community) doi:10.1895/wormbook.1.142.1, <http://www.wormbook.org> (2008).
48. Li, C., Nelson, L.S., Kim, K., Nathoo, A. & Hart, A.C. Neuropeptide gene families in the nematode *Caenorhabditis elegans*. *Ann. NY Acad. Sci.* **897**, 239–252 (1999).
49. Kindt, K.S. *et al.* Dopamine mediates context-dependent modulation of sensory plasticity in *C. elegans*. *Neuron* **55**, 662–676 (2007).

ONLINE METHODS

Calcium imaging. To generate an AIA imaging line, GCaMP2.2b (ref. 15) was expressed under the *gcy-28.d* promoter[8], which is expressed strongly in AIA neurons and weakly in RIA, ASK, AVJ and other cells. The AWC GCaMP1 imaging line has been described[9]. The lines were scored quantitatively for AWC local search behaviors, and those with normal responses were used for calcium imaging. Worms were trapped in a custom-designed microfluidic device made of the transparent polymer PDMS in which animals are restrained in a small chamber matching their dimensions, exposed to odors in liquid streams under laminar flow, and monitored using wide-field fluorescence microscopy[9,22]. Fluorescence from the cell of interest was captured after the presentation of isoamyl alcohol (10^{-4} dilution) and after odor removal 5 min later.

We used MetaMorph and a Coolsnap HQ (Photometrics) camera to capture stacks of TIFF images at 10 frames s^{-1} during the addition and removal of odor stimulus. A region of interest encompassing the cell was identified in all frames and the average fluorescence intensity recorded. A Matlab (7.0R14, MathWorks) script used the data generated by MetaMorph to plot the imaging responses. The average fluorescence of the region of interest was generated by subtracting the recorded value from the average intensity of the background region of a similar area. The average fluorescence in a 3-s window (t = 1–4 s) was set as F_o. The percent change in the fluorescence intensity for the region of interest relative to F_o was plotted for all stacks, and these data were used for further analysis. Raw traces were corrected for fluorescence bleaching by subtracting a fixed correction function obtained by fitting an exponential curve to wild-type control traces using the equation $y(t) = 100\%\ [\exp(-t/\tau) - 1]$ where t is time and τ is the time constant. As bleaching rates varied among neurons, separate time constants were obtained for AWC (τ = 330.7 s; 95% confidence interval, 327.1–334.4 s; $R^2 = 0.91$) and AIA (τ = 615.5 s; 95% confidence interval, 607.2–623.8 s; $R^2 = 0.86$).

Because the irregular secondary calcium transients in AWC were not visible in averaged traces, we plotted the ratio of change in fluorescence to total fluorescence for individual traces in heat maps in **Figure 3** and **Supplementary Figures 1** and **4**. The wild-type controls for each figure were interleaved with mutants tested over the same time period.

Local search behavior. Individual worms were scored for exploratory behavior in the presence of food (5 min), immediately after removal from food (1–12 min) and after long times off food (35–40 min)[6,9]. All turns and reversals were scored by eye, by an investigator blind to the genotype of the worm. Reversals and turns were identified as described[6]. Results in **Figures 1** and **5** show turning rates scored 7–12 min after removal from food, and are reported as RevOmega values, which represent reversals coupled to omegas. Qualitatively similar results were obtained when large reversals or omega turns were scored individually (**Supplementary Table 1**). Data were analyzed using Perl scripts to calculate reversal and omega frequencies.

Adaptation assays. Adaptation assays were performed as described[26]. Worms were washed and plated on 3% assay agar plates. We placed 16 µl of isoamyl alcohol on agar plugs on the plate lid and sealed the plates with Parafilm to create the conditioning plate. After 60 min or 90 min, worms were washed and tested for chemotaxis on fresh plates. Controls were treated identically except that isoamyl alcohol was omitted from the conditioning plate. For imaging experiments, worms were conditioned for 60 min with or without isoamyl alcohol and then loaded into the device for calcium imaging.

Discrete Fourier transform. The plots in **Figures 3d,h** and **5b** and **Supplementary Figures 1** and **4d** were generated by transforming data in the time domain (the raw fluorescence trace $y(t)$) into the frequency domain ($Y(f)$), using the Matlab function fft (discrete Fourier transform), which computes

$$Y(f_k) = \sum_{j=0}^{N-1} y(t_j) e^{\frac{-2\pi i}{N} kj} \quad (1)$$

where k = 0 … N – 1, N = 1,200 and $i = \sqrt{-1}$

at 1,200 equally spaced frequencies from f0 = 0 to f1199 = 10 Hz, the sampling rate. Aliasing, or contribution from oscillatory components at higher than the Nyquist frequency (5 Hz), is negligible based on the rapid drop-off of the Fourier transform with increasing frequency because the dynamics of calcium fluorescent indicators is slower than the sampling rate. The normalized energy spectral density, $|Y(f_k)|^2 \Big/ \sum_{f_1 \le f_k \le f_{N/2}} |Y(f_k)|^2$, was then calculated for each trace and averaged across each group of traces at each f_k sample point to give $\left\langle |Y(f_k)|^2 \Big/ \sum_{f_1 \le f_k \le f_{N/2}} |Y(f_k)|^2 \right\rangle_{\text{trials}}$ versus f_k (**Figs. 3d,h** and **5b**). The value $|Y(f_0)|$ represents the mean of the entire time-domain vector $y(t)$ and was excluded from the calculation of energy spectral density normalization and band power ratio (described below), although including the value in the calculations did not significantly affect results. Values of $f > f_{N/2}$ were also excluded from calculations owing to the redundancy of the magnitude of the second half of the discrete Fourier spectrum when performed on real-valued signals. For simplicity, no smoothing or windowing was applied to the energy spectral density. Applying various windowing schemes did not significantly affect quantifications (data not shown).

This representation of calcium signal data was chosen for two reasons. First, because calcium events were not registered in time, transients after the initial peak response were typically lost when averaging traces from multiple worms (**Supplementary Fig. 2a**,**b**). By contrast, the frequency-domain representation separates magnitude and phase information and secondary transients are preserved when averaging over many experiments. Second, this representation allows the identification and separation of signal components in various frequency bands. Low frequencies capture the magnitude of the primary response, high frequencies capture signal measurement noise, and middle frequencies capture secondary transients.

As an estimate of the portion of the total signal contributed by oscillatory components in a band bounded by two frequencies $f_{\min}$ and $f_{\max}$, we compute the band power ratio as

$$\text{Band power ratio}(f_{\min}, f_{\max}) = \sum_{f_{\min} \le f_k \le f_{\max}} |Y(f_k)|^2 \Big/ \sum_{f_1 \le f_k \le f_{N/2}} |Y(f_k)|^2 \quad (2)$$

The complete time domain trace $y(t)$ can be exactly reconstructed from its complex Fourier spectrum using the inverse discrete Fourier transform (Matlab function ifft), which computes:

$$y(t_j) = \frac{1}{N} \sum_{k=0}^{N-1} Y(f_k) e^{\frac{2\pi i}{N} kj} \quad (3)$$

where j = 0 … N – 1, N = 1,200 and $i = \sqrt{-1}$

To visualize signal contributions from each frequency band, we divided Fourier spectra into three frequency bands, and reconstructed time-domain signals represented by the contributions from a single frequency band using the inverse discrete Fourier transform (equation (3)) of the complex Fourier spectrum clipped to zero everywhere outside of the particular frequency band. Middle band reconstructions are shown in **Supplementary Figures 1** and **4d**. By mathematical identity, the sum of the low, middle and high-frequency trace reconstructions equals the full time-domain fluorescence trace. As reconstructions based on sharply clipped samples can result in ringing effects (continued oscillations during a time period when the original trace is not oscillating), we also performed reconstructions using sloped frequency windows. No important changes in the appearance of trace reconstructions during the 30–120-s period were observed (not shown).

The choice of middle frequency band range was made by separating the Fourier spectra into many bands (10 cutoffs, at 0.001, 0.01, 0.02, 0.033, 0.1, 0.2, 0.5, 1, 2 and 5 Hz) and selecting the bands that significantly distinguished wild-type from *nlp-1* responses (data not shown). We found that most *nlp-1* secondary transients are captured in a narrower, f = 0.033–0.2 Hz band, but *nlp-1* traces also show increased oscillation in the f = 0.2–1 Hz range; hence, we selected the combination of these bands (f = 0.033–1 Hz) as the region of interest for **Supplementary Figures 1** and **4d**. This frequency range corresponds to periodic oscillations with periods between 1 and 30 s. The different genotypes did not show significant differences in the frequency domains <0.033 Hz or >1 Hz, suggesting little effect on the primary response or signal noise.

Three of the genotypes (*nlp-1*, *npr-11* and *ins-1*) showed strong secondary calcium transients. The *nlp-1* energy spectral density shows a broad peak in frequency-domain amplitude at f = 0.0583 Hz (**Fig. 3d**), corresponding to a period

doi:10.1038/nn.2526

of 17 s; this period is similar to the time period between large calcium transients determined by a manual measurement of *nlp-1* traces (19.5 ± 2.2 s (mean ± s.d.); **Fig. 3b**). Similarly, *npr-11* and *ins-1* worms show increased amplitude at frequencies corresponding to a period between 10 and 20 s (**Fig. 3f**,**h** and **Supplementary Fig. 4b**,**d**). These transients were not observed during imaging of wild-type or *nlp-1* worms during buffer exchange protocols (**Supplementary Fig. 1**). All calculations were performed with Matlab.

Cell culture and calcium imaging. Two peptides, one corresponding to the NLP-1 sequence (MDANAFRMSFamide) and the second with a scrambled sequence (MSMRFANADFamide), were synthesized by the Proteomics resource center at The Rockefeller University. Human embryonic kidney 293 cells (HEK293) were cultured in DMEM supplemented with 10% FBS at 37 °C in a humidified atmosphere containing 5% CO_2. Cells 50–60% confluent were transfected with a 1:1 ratio of pME18s-*npr-11* and pcDNA3-α16Z (encoding a promiscuous G protein[13], a gift from Y.H. Wang) using Lipofectamine 2000 and incubated for at least 24 h; the transient transfection efficiency was ~70%, estimated by cotransfecting β2-adrenergic receptor and Gα15 plasmids and counting the fraction of cells responsive to isoproterenol. In control experiments, the receptor or G protein was transfected alone. Experiments were conducted on three plates for each condition on three different days. The transfected cells were loaded with 2.5 μM fura-2/AM for 20 min at 37 °C, peptide solution was applied sequentially to the cells for 15 s with a peristaltic pump, and fluorescence at 510 nm by excitation at 340/380 nm was monitored using a MetaFluor calcium imaging system. The calcium response trace was calculated using all cells in randomly chosen fields. For receptor and G protein transfections, ten fields were analyzed, for G protein alone, seven fields, and for receptor alone, eight fields.

Laser ablations. In transgenic worms expressing GCaMP2.2b under an AIA-specific promoter, AWC neurons were identified based on their position and morphology using Nomarski optics, and killed with a Micropoint laser system. Operated worms were tested in parallel with controls from the same strain on the same day.

Molecular biology and transgenesis. cDNA or genomic regions corresponding to the entire coding sequences of *nlp-1*, *npr-11* and *ins-1* were amplified by PCR from mRNA or genomic DNA and expressed under cell-specific promoters as indicated. For behavioral experiments in transgenic lines, a splice leader (SL2) fused to a *gfp* transgene was used to confirm cell-specific expression of the gene of interest, and only worms expressing GFP were scored. Selective expression in AWC, ASI, AIA or AIY was achieved using the promoters *odr-3* (AWC>AWB), *str-3* (ASI alone), *gcy-28.d* (AIA) and *ttx-3* (AIY alone). Germline transformations were carried out my microinjection of plasmids at concentrations between 10 and 50 ng μl^{-1}. Strains were grown and maintained under standard conditions[50].

50. Brenner, S. The genetics of *Caenorhabditis elegans*. *Genetics* **77**, 71–94 (1974).